Measurement 227 (2024) 114259

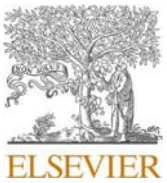

Contents lists available at ScienceDirect

Measurement

journal homepage: www.elsevier.com/locate/measurement

Photoacoustic spectroscopy for fault diagnostics in high voltage power transmission systems: A review

Qianhe Wei [a,b,c], Bincheng Li [a,*], Binxing Zhao [a], Ping Yang [b], Lei Dong [d]

[a] School of Optoelectronic Science and Engineering, University of Electronic Science and Technology of China, Chengdu 610054, China
[b] Institute of Optics and Electronics, Chinese Academy of Sciences, Chengdu 610209, China
[c] University of Chinese Academy of Sciences, Beijing 100049, China
[d] State Key Laboratory of Quantum Optics and Quantum Optics Devices, Institute of Laser Spectroscopy, Shanxi University, Shanxi 030006, China

ARTICLE INFO

Keywords:
Photoacoustic spectroscopy
Trace gas detection
Oil-immersed power transformer
SF_6 insulated equipment
Insulation defect

ABSTRACT

The diagnosis of incipient faults in high-voltage power transmission equipment is vital to the normal operation of the power grid. Monitoring the contents and variation trends of the decomposition gases is a diagnostic method widely used to determine incipient faults. Photoacoustic spectroscopy (PAS), with the advantages of fast response time, compact structure, strong anti-interference ability, and real-time and in-situ monitoring, is an effective technique to detect decomposition gases for fault diagnostics of high-voltage power transmission systems. In this review, a brief introduction to PAS's theoretical background and system requirements is first described. Subsequently, a detailed summary of the recent applications of PAS to high-voltage power transmission systems, with a focus on fault diagnosis in both oil-immersed power transformers and SF_6-insulated equipment, is provided. Finally, PAS perspectives for using decomposition gas analysis to monitor faults in high-voltage power transmission lines are discussed.

1. Introduction

Electrical power systems are networks of electrical components employed to supply, transfer, and use power, consisting of power generators, power transmission systems, and distribution systems [1]. Power transmission systems, as indispensable parts, transmit electricity from power generation centers to load centers. High-voltage power transmission systems play a significant role in current power systems due to that a higher voltage in a transmission line greatly improves transmission efficiency. Knowing the status and conditions of power equipment is essential to the stability and security of high-voltage power transmission systems and prevents substantial capital losses [2]. Therefore, ensuring the health and proper operation of high-voltage power equipment is essential. However, due to manufacturing or operational imperfections, the equipment inevitably experiences faults such as discharge and overheating during operation [3]. Most power equipment faults are diagnosed on the basis of electrical, physical, and chemical parameters [4]. Electrical tests, like insulation resistance and partial discharge analysis, provide immediate insights but may not detect subtle faults and risk equipment damage. Physical methods such as thermal imaging and vibration analysis are effective for operational health checks but require specialized interpretation and can be impeded by external environment influences [5–7]. Chemical parameter testing is vital for diagnosing faults in insulation equipment and essential for the stable operation of high-voltage power transmission systems and their safety and reliability [8,9]. This method can effectively and conveniently analyze the chemical composition of the insulating medium, enabling early fault detection and offering a detailed, preemptive understanding of equipment condition. The decomposition gas analysis method is a chemical detection method with the advantages of non-intrusiveness and protection from harmful electrical interference [10]. It is widely applied in power systems to diagnose insulation faults such as oil-immersed power transformers and SF_6-insulated equipment [11,12]. Fault detection in these types of equipment relies on identifying various decomposition gases produced due to distinct defects [13]. These gases manifest at different generation rates and concentrations, depending on the defect nature. Consequently, the simultaneous and precise measurement of multiple decomposition gases is crucial for the prompt and accurate identification of faults in high-voltage electrical equipment.

Currently, some traditional gas sensors have been developed to meet some of these applications, mainly including gas detection tubes [14], gas chromatography-mass spectrometry (GC–MS) [15], and Fourier transform infrared spectroscopy (FTIR) [16]. The operation of the gas

* Corresponding author.

https://doi.org/10.1016/j.measurement.2024.114259
Received 28 October 2023; Received in revised form 15 January 2024; Accepted 29 January 2024
Available online 2 February 2024

detection tube is simple, but it is vulnerable to factors such as temperature, humidity, and storage duration. GC–MS is capable of detecting gases with multiple compositions and has a high detection limit ranging from parts-per-trillion (ppt) to parts-per-billion (ppb). However, it is expensive, requires tedious sample collection, involves a complex preconcentration process, and is larger in size. As a result, it is primarily used for laboratory testing rather than continuous online monitoring or onsite testing. FTIR detects trace gases with high resolution and fast response. However, it has the drawback of consuming a large amount of sample due to the long optical path length, as well as the interference between different gases in the infrared spectrum. Additionally, its limited spectral resolution restricts its use in industrial settings. In contrast, laser absorption spectroscopy detection techniques like tunable diode laser absorption spectroscopy (TDLAS), photoacoustic spectroscopy (PAS), and cavity ring-down spectroscopy (CRDS), with advantages of fast response, high sensitivity, high selectivity, high long-term stability, and real-time and in-situ monitoring capability, have reached a mature state. PAS does not directly quantify the attenuation of light, but instead detects the acoustic signal produced as a result of the absorption of light by the gas being measured [17]. Consequently, the presence of a photodetector in PAS is unnecessary, so the choice of wavelength for the light source remains unaffected by the detector. The sensitivity of the PAS system is not affected by the length of the gas-laser interaction, ensuring a compact setup of the system. Currently, PAS has been implemented across various domains, and the minimum detectable gas concentration has achieved ppt or even sub-ppt level [18]. The applications of PAS on the identification of some decomposition gases in high-voltage power transmission systems have also received widespread attention.

There is a recent publication that reviewed the applications of PAS in fault diagnostics of gas-insulated switchgears, in which PAS detections of SF_6 decomposition gases CO, SO_2, CF_4, and H_2S were summarized, but without the detections of two other major decomposition gases, SO_2F_2 and SOF_2 [19]. This review provides a detailed examination of the applications of PAS in fault diagnostics for both oil-immersed power transformers and SF_6-insulation equipment, with detections of additional decomposition gases. The review commences with an exploration of the theoretical background of PAS, followed by a brief overview of PA systems, encompassing light sources, light modulation, PA cells, and PA detectors. The concluding section offers a comprehensive summary of the recent applications of various PAS types in fault diagnostics for both oil-immersed power transformers and SF_6-insulated equipment.

2. Basic principle of photoacoustic spectroscopy

In 1880, A.G. Bell discovered that modulated light can excite acoustic signals in solids, known as the PA effect, which was then introduced into the field of gas detection [20]. The essence of the PA effect lies in the conversion of optical radiation to sound [21], as illustrated in Fig. 1, depicting the generation and detection of sound in gas. Through an absorption process, gas molecules go from a low-energy state to an excited state (vibrational, rotational, or electronic quantum state) when modulated or pulsed light at a certain wavelength interacts with the gas sample. The temperature and pressure of the gas increase as a result of the excited state molecules releasing energy through a non-radiative relaxation mechanism that converts vibrational energy into translational (kinetic) energy of gas molecules. An acoustic signal is produced when temperature and pressure changes as a result of the stimulating light source's periodic modulation. This causes the gas inside an enclosed chamber to expand and contract. Ultimately, the sound signal produced is detected by the sound sensor, and the resulting electrical signal is evaluated to extract pertinent information about the gas sample.

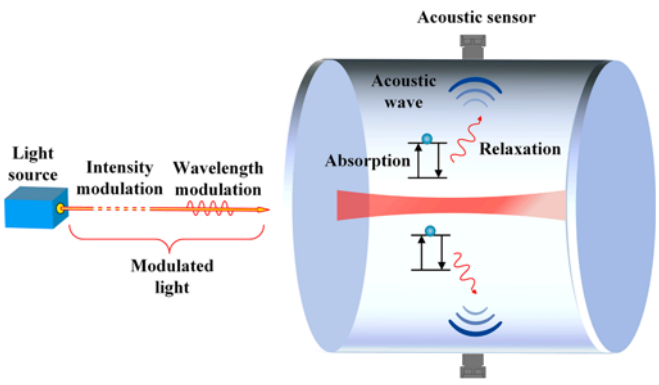

Fig. 1. The processes of PA signal generation.

In the absence of saturation (saturation effect will occur when laser energy and gas concentration are excessive), PA signals can be expressed as follows [22]:

$$S \propto \frac{Q \cdot P \cdot N \cdot \sigma}{f} \tag{1}$$

where P is the incident optical power, f is the resonant frequency, Q is the quality factor of the acoustic resonator, N is the total number density of molecules, and σ is the absorption coefficient. According to Eq. (1), there are three primary approaches to enhancing PA signals: the selection of high-power lasers, the selection of a wavelength range with a high absorption intensity, and the change in the size of the acoustic resonator and acoustic sensor to achieve a higher Q/f ratio.

To compare the performance of different PAS systems, the minimum detectable concentration $c_{\min}$ can be an important criterion, expressed as Eq. (2) [23]:

$$c_{\min} = \frac{\alpha_{\min}}{noise \cdot \sigma} \tag{2}$$

where $\alpha_{\min}$ is the minimum absorption coefficient (in cm^{-1}) determined when the PA signal is equal to the noise (signal-to-noise ratio $SNR = 1$). Commonly, one or three times the noise standard deviation value is used to indicate the noise. Another indicator for comparing various PAS systems is normalized noise equivalent absorption (*NNEA*) [24], providing a common basis for comparing various PAS systems, which can be determined by Eq. (3):

$$NNEA = \frac{\alpha_{\min} P}{\sqrt{\Delta f}} \tag{3}$$

where Δf is the equivalent noise detection bandwidth.

PA gas detection systems generally consist of a light source, an optical modulation module, a gas cell, an acoustic sensor, and a signal demodulation module. Light sources are classified as non-coherent (blackbody radiators and light emitting diodes) and coherent (lasers) based on their radiation properties. When measuring decomposing gases with an incoherent light source, different narrowband filters are frequently needed, which reduces spectral resolution and makes it more difficult to discriminate distinct gases with cross-interfering absorption signatures [25]. The most widely used coherent light source in PAS is a distributed feedback (DFB) diode laser, which has the advantages of compactness, robustness, low cost, and long service lifetime. Nevertheless, their functionality is limited to the near-infrared (IR) spectrum, which exhibits absorption line strength that is 2–4 orders of magnitude lower compared to the mid-infrared band. Consequently, an optical fiber amplifier device is necessary to augment their output power. Moreover, the restricted tunable range of the laser necessitates the use of numerous lasers in multi-gas PA detection systems, hence augmenting their intricacy. Another commonly used coherent light source is a quantum cascade laser (QCL), which has significant dominance in the mid-IR spectral region. QCL can achieve a tunable range of a few microns and an output power of several watts, but this requires the use of water

cooling to effectively dissipate heat.

There are two leading modulation techniques, namely intensity modulation and wavelength modulation [22]. In intensity modulation the amplitude of incident radiation is modulated via mechanical choppers, electro-optic modulators, or acousto-optic modulators. The intensity modulation technique is primarily used to detect polyatomic gas molecules (SF_6, SO_2F_2 and CF_4), which usually have IR absorption spectral range exceeding 100 cm^{-1} [26]. However, PAS is no longer a background-free technique since noise with the same frequency as the target PA signal will be produced when the intensity-modulated light irradiates the cavity mirror and the PA cell wall. Therefore, in order to obtain the PA signal of the target gas, it is usually necessary to subtract the background signal via vector subtraction [27]. The wavelength modulation technique alters the frequency of the laser periodically by modulating the injection current of the laser with a sine wave. Since the PA effect of the gas is selective to wavelength, a PA signal generated by the gas analyte absorbing light of a specific wavelength can be obtained. This PA signal can be distinguished from the constant background noise caused by the absorption of the PA cell wall and cavity mirrors, which is not dependent on wavelength. Wavelength modulation is invariably used in combination with second harmonic detection. In recent years, wavelength modulated PAS has been widely used to achieve higher SNRs for molecules with narrow absorption lines due to its background-free nature [28]. Modulation signals can be demodulated using digital lock-in amplifier or Fourier transform. Typically, intensity-modulated signals are demodulated at the resonant frequency, whereas wavelength-modulated signals are demodulated at the second harmonic.

An ideal PA cell should have the characteristics of amplifying an acoustic signal while avoiding the generation of noise, a small volume for low consumption of sample gas, and no absorption of incident light by other materials [29]. Modifying the structure and dimensions of the PA cell can alter the resonance mode of the acoustic wave. So far, different types of PA cells have been suggested [30], including H-type one-dimensional resonant PA cells with two buffers that prevent flow noise and window background signals, differential PA cells that can double signal amplitude and greatly reduce external acoustic noise, and Helmholtz resonant PA cells with higher sensitivity at lower modulation frequencies.

The acoustic sensors of PAS applied to fault diagnostics in high-voltage power transmission systems mainly include capacitive microphones, quartz tuning forks and optical microphones. Capacitive microphones that convert an acoustic signal into an electric signal are widely employed in PAS. The benefits of the capacitive microphone are its low cost, robustness, reliability, and wide frequency range [31]. Unfortunately, the electrical signal generated by the capacitive microphones is very weak and usually needs to be combined with a preamplifier, which limits the development of PAS miniaturization. Additionally, capacitive microphones are susceptible to electromagnetic interference and temperature variations, limiting their applications. The QTF, a highly advancing acoustic sensor, has gained prominence in recent years. It operates by utilizing piezoelectricity to detect vibration pressure on its tip and then converts the sound wave into an electrical signal for detection. This eliminates the need for acoustic resonance conditions in the design of PA cells [32]. The QTF-based PAS is referred to as quartz-enhanced photoacoustic spectroscopy (QEPAS). QTF is usually combined with an acoustic micro resonator (AmR) to achieve signal enhancement. The term used to describe PAS that utilizes an optical microphone for detecting sound is all-optical PAS. Optical microphones employ various optical techniques, including as intensity modulation, fiber Bragg grating, and interferometry, to detect changes in the surface of the diaphragm or cantilever generated by sound waves. This allows for the measurement of information about the gas being analyzed [33]. Due to the absence of electronic components in the conversion process from acoustic to optical signals, the all-optical PAS is immune to high temperatures and electromagnetic interference [34]. Nevertheless, the measurement precision of the all-optical PAS is susceptible to any environmental vibrations, making it unsuitable for environments with significant vibration.

3. Applications of PAS to fault diagnostics in oil-immersed power transformers

3.1. Fault diagnosis of oil-immersed power transformers

Currently, large oil-immersed power transformers remain prevalent in high-voltage transmission systems, favored for their capacity to manage higher voltage levels compared to dry-type transformers [35]. As essential and expensive components of the transmission and distribution networks, they play a crucial role in ensuring that consumers receive electrical energy at the appropriate voltage levels [36,37]. Therefore, maintaining transformers in good condition is crucial for system reliability. The fundamental causes of transformer faults can be categorized into electrical, thermal, and mechanical factors, or a combination of these, as illustrated in Fig. 2 [38]. Over the years, a variety of sensor technologies have been developed for power transformer condition monitoring, capable of being used in both online and offline fault diagnosis (Fig. 3) [39–43].

Dissolved gas analysis (DGA) is a widely utilized diagnostic approach employed by major electrical firms and transformer manufacturers worldwide [10,44]. DGA is essential for effective transformer health monitoring and maintenance planning [45]. In order to evaluate and identify different forms of transformer problems, it entails analyzing gases dissolved in the transformer oil in conjunction with many systems [46]. As a diagnostic tool in oil-immersed transformers, DGA detects gases produced by electrical and thermal stress in the insulating oil [47]. The presence and concentration of these gases indicate different types of internal faults, aiding in early detection of issues like overheating, arcing, or insulation breakdown. For example, if overheating fault only occurs in the insulating oil, the characteristic decomposition gas is mainly CH_4 and C_2H_4. However, when it is present in both solid insulation materials and insulating oil, CO_2 and CO are also produced [48]. The key gases liberated from the transformer insulating materials and their corresponding faults are summarized in Table 1. The permissible levels of decomposition gases in the oil of regular oil-immersed power transformers are as follows: H_2 (100 ppm), C_2H_6 (65 ppm), CH_4 (120 ppm), C_2H_2 (35 ppm), C_2H_4 (50 ppm), CO (350 ppm), and CO_2 (2500 ppm) [49]. Currently, there are several DGA interpretation methods, including key gas analysis, nomograph method, dornenberg and rogers ratio method, CIGRE method, duval triangle method, and IEC ratio method. Research indicates that DGA can detect and provide alarms for about 70% of power transformer problems, despite the fact that these techniques are based on empirical assumptions drawn from lab results [50–53]. For precise interpretation of DGA data, it is crucial to have accurate gas detection. Nowadays, PAS based online DGA monitoring plays an essential role in dissolved gas detection. Since most gas molecules have strong absorption in the mid-IR and near-IR spectral regions, PAS detection of oil-dissolved gases (C_2H_6, CH_4, C_2H_2, C_2H_4, CO, CO_2) is mainly in the mid- and near-IR wavelength ranges. According to the HITRAN database [54], absorption spectra of oil-dissolved gases in the mid- and near-IR are shown in Fig. 4(a) and (b), respectively. In the following sections, the research on PAS in oil-immersed power transformers in recent years is summarized according to the different types of PAS, and are listed in Tables 2 and 3 according to single-gas and multi-gas detection, respectively, for easy reference.

3.2. PAS for fault diagnosis of oil-immersed power transformers

3.2.1. Traditional photoacoustic spectroscopy

Traditional PAS systems employ different types of PA cells equipped with capacitive microphones for the amplification and detection of acoustic signals. Wu et al. developed a second harmonic PAS system using a tunable erbium-doped fiber laser (TEDFL) operating at

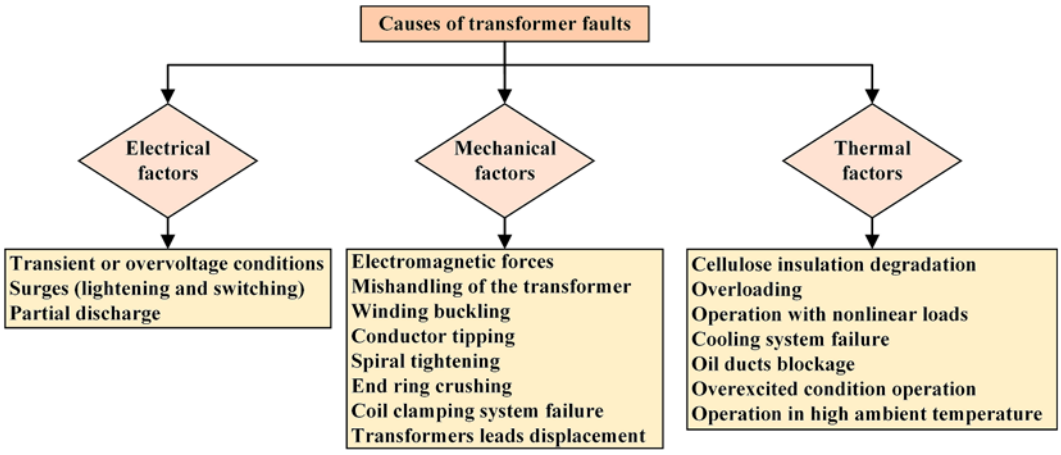

Fig. 2. Causes of faults in oil-immersed transformers.

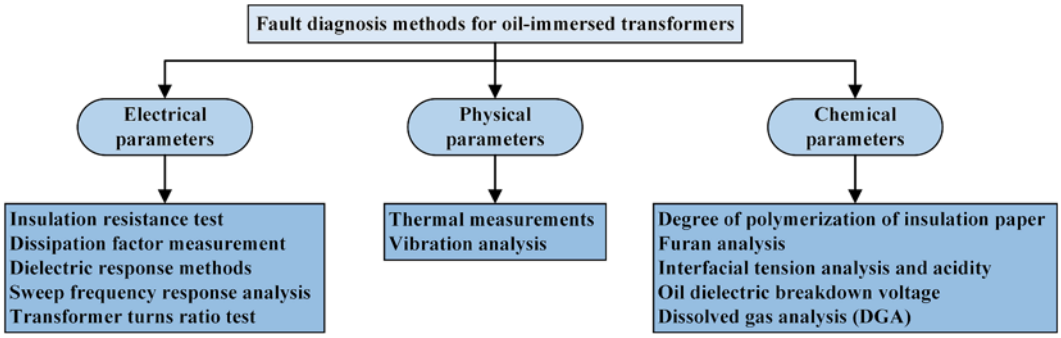

Fig. 3. Fault diagnosis methods for oil-immersed power transformers.

Table 1
The key gases and their corresponding fault.

Fault type	Major gas	Minor gas
Oil overheating	C_2H_2, CH_4	C_2H_6, H_2
Oil and paper overheating	C_2H_4, CH_4, CO, CO_2	C_2H_6, H_2
Partial discharge in oil-paper insulation	CH_4, H_2, CO	C_2H_2, CO_2, C_2H_6
Spark discharge in oil	C_2H_2, H_2	/
Electric arc in oil	C_2H_2, H_2	C_2H_4, CH_4, C_2H_6
Electric arc in oil paper	H_2, CO, C_2H_2, CO_2	C_2H_4, CH_4, C_2H_6
Moisture	H_2	/

approximately 1530.3709 nm. They combined this with an H-type one-dimensional resonant PA cell to detect three dissolved gases and the interfering gas H2O in insulating oils simultaneously [55]. To effectively extract the characteristic PA signals corresponding to the central wavelengths of the four gases, a blind source separation (BSS) analysis model was proposed. This model is based on overcomplete independent component analysis (ICA) and the FastICA analysis algorithm, which incorporates a weight truncation constraint equation to address the cross-interference in the absorption characteristics of the gases. In addition, this algorithm is primarily suitable for the extraction of mixtures of gas components with super-Gaussian distributions of lines in the near IR. Ma et al. employed an erbium-doped fiber amplifier to enhance the optical output of a near-infrared DFB diode laser to 1 W in order to counterbalance the weak absorption intensity of C_2H_2 [56]. Using a multi-pass retro-reflection-cavity-enhanced PA cell (Fig. 5) based on a one-dimensional H-type resonant PA cell, two right-angle prisms allow the laser to pass through the PA cell four times, which significantly enhances the PA signal of C_2H_2. Wang *et al.* designed a T-type PA cell for detecting dissolved C_2H_2 in oil. In contrast to the H-type PA cell, the T-type PA cell has only one buffer chamber, and the capacitive microphone is located at one end of the resonant tube, rather than in the middle [57]. Although the fundamental features of the two PA cells are nearly indistinguishable, the T-type PA cell has a smaller volume compared to the H-type PA cell, resulting in a decreased usage of sample gas. In a study by Li *et al.*, they proposed the development of a high-sensitivity multi-pass absorption-enhanced PA system based on an infrared broadband light source and two DFB lasers for the detection of six dissolved gases in oil [58]. The concave mirror with holes at one end and a BaF_2 window at the other is features of the cylindrical PA cell. The mid-IR radiation source with four filters used to detect C_2H_6, C_2H_4, CO, and CO_2 is reflected once by a concave mirror, which creates a double-pass absorption enhancement. The two DFB lasers used to detect CH_4 and C_2H_2 are incident into the PA cell from the small hole opened on the concave mirror through a fiber wavelength division multiplexer (WDM) coupling. The plane mirror and concave mirror create a chamber in which the two DFB lasers bounce back and forth several times, greatly enhancing the PA signal and ultimately achieving ppm levels of detection sensitivity (Fig. 6).

3.2.2. *Quartz enhanced photoacoustic spectroscopy*

Ma et al. conducted high-sensitivity detection studies on C_2H_2 trace gas using on-beam QEPAS [59], as shown in Fig. 7. As an alternative to the common QTF with a resonance frequency of 32768 Hz, a QTF with a lower resonance frequency of 30720 Hz was used as the acoustic microphone in order to enhance the signal amplitude of the system. The acoustic signal is further enhanced by adding a micro resonator to both ends of a QTF in order to form a standing wave under the action of the micro resonator, which increases the PA signal by approximately 8 times as a result. The minimum detection limit and the normalized noise equivalent absorption coefficient of the system were calculated to be 2.7 ppm and $1.3 \times 10^{-8}\,\mathrm{Wcm^{-1}Hz^{-1/2}}$, respectively. As an alternative to the

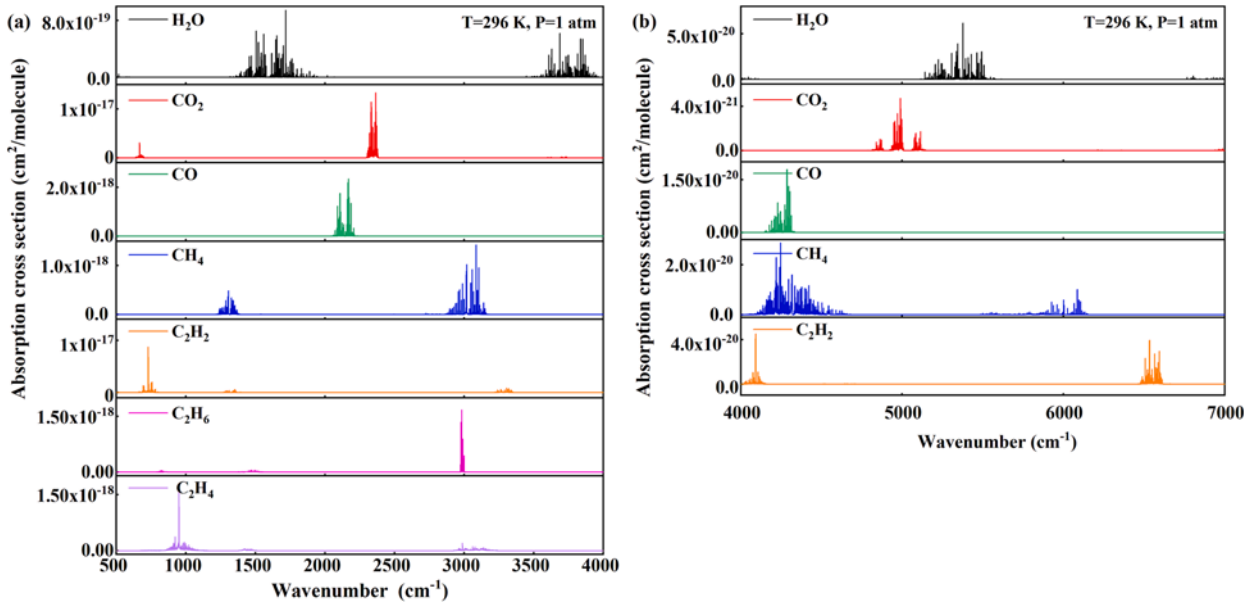

Fig. 4. Absorption spectra of oil-dissolved gases and water vapor in the mid-IR (a) and near-IR (b).

Table 2
Applications of PAS to single-gas detection in oil-immersed power transformers.

Gas	Light source	Acoustic sensor	Wavelength	Detection limit	Integration time	Ref.
CO	DFB laser	Capacitive microphone	1567 nm	/	1 s	[64]
	DFB laser	Capacitive microphone	1567 nm	/	1 s	[65]
C_2H_2	TEDFL	Optical microphone	1531.59 nm	0.87 ppb	1 s	[66]
	TEDFL	Optical microphone	1530.37 nm	1.56 ppb	100 ms	[60]
	DFB laser	Optical microphone	1532.83 nm	6 ppb	1 s	[67]
	DFB laser	Capacitive microphone	1532.83 nm	/	1 s	[57]
	DFB laser	Optical microphone	1529.78 nm	4.3 ppm	10 s	[68]
	DFB laser	Capacitive microphone	1532.83 nm	12.2 ppb	400 s	[69]
	DFB laser	Optical microphone	1532.83 nm	119 ppt	60 s	[70]
	DFB laser	Optical microphone	1532.8 nm	50 ppb	1 s	[71]
	Digital supermode DBR (DS-DBR) laser	Optical microphone	1530.37 nm	0.047 ppm	300 ms	[72]
	DFB laser	/	1532.84 nm	3.4 ppb	/	[73]
	DFB laser	Optical microphone	1532.83 nm	1.47 ppb	1 s	[74]
	DFB laser	/	1531.58 nm	7 ppb	154 s	[75]
	DFB laser	Capacitive microphone	1532.83 nm	0.37 ppb	60 s	[76]
	IR radiation source	Optical microphone	3073 nm	8 ppb	80 s	[77]
	DFB laser	QTF	1530.37 nm	2.7 ppm	1 s	[59]
	DFB laser	Optical microphone	1532.83 nm	71 ppt	200 s	[63]
	DFB laser	Capacitive microphone	1530.37 nm	600 ppt	1000 s	[56]
	DFB laser	Optical microphone	1532.83 nm	0.7 ppb	/	[78]
CH_4	IR radiation source	/	/	6.9 ppm	/	[79]
	DFB laser	Optical microphone	1651 nm	15.9 ppb	1000 s	[62]
	DFB laser	Optical microphone	1650.96 nm	9 ppb	500 s	[80]
	DFB lasers	/	1654 nm	/	1 s	[81]
	Near-IR Laser	Optical microphone	1653.67 nm	130 ppb	10 s	[82]

common QTF with a resonance frequency of 32768 Hz, a QTF with a lower resonance frequency of 30720 Hz was used as the acoustic microphone in order to enhance the signal amplitude of the system. By adding a micro resonator at both ends of a quartz tuning fork (QTF), the acoustic signal is significantly amplified, leading to the formation of a standing wave. This interaction with the micro resonator results in an approximate eightfold increase in the PA signal. The minimum detection limit and the normalized noise equivalent absorption coefficient of the system were calculated to be 2.7 ppm and 1.3 × 10^{-8} $Wcm^{-1}Hz^{-1/2}$, respectively.

3.2.3. *All-optical photoacoustic spectroscopy*

Based on a phthalazinone ether sulfone ketone (PPESK) diaphragm, Wang *et al.* demonstrated a highly sensitive extrinsic Fabry-Perot interferometer (EFPI) fiber acoustic sensor for C_2H_2 detection [60]. The interferometer was utilized to quantify the minute alteration in optical path induced by the acoustic pressure exerted on the diaphragm. The EFPI acoustic sensor was placed in the middle of the H-type resonator. The minimum detection limit of ppb level has finally been reached. Gong *et al.* used a Parylene-C diaphragm with a thickness of 800 nm and an inner diameter of 9 mm along with a fiber-tip Fabry-Perot interferometer as the acoustic sensor [61]. A non-resonant cylindrical PA cell operating at a frequency of 30 Hz and an IR thermal

Table 3
Applications of PAS to multi-gas detection in oil-immersed power transformers.

Light source	Acoustic sensor	Integration time	Wavelength	Gas	Detection limit	Ref.
TEDFL	Capacitive microphone	/	1530.3709 nm	C_2H_2	/	[55]
			1530.3872 nm	CO_2	/	
			1530.3608 nm	CH_4	/	
			1530.3675 nm	H_2O	/	
TEDFL	Capacitive microphone	/	1531.59 nm	C_2H_2	4 ppb	[83]
			1565.98 nm	CO	39 ppm	
			1572.34 nm	CO_2	34 ppm	
IR radiation source	Optical microphone	/	3050 nm	C_2H_2	0.11 ppm	[61]
			3220 nm	CH_4	0.21 ppm	
			3374 nm	C_2H_6	0.13 ppm	
			10,688 nm	C_2H_4	0.16 ppm	
			4685 nm	CO	0.15 ppm	
			4266 nm	CO_2	0.48 ppm	
DFB laser	Capacitive microphone	60 s	1532.83 nm	C_2H_2	27 ppb	[84]
IR radiation source			3220 nm	CH_4	24 ppb	
			3370 nm	C_2H_6	20 ppb	
			10,690 nm	C_2H_4	39 ppb	
			4690 nm	CO	10 ppb	
			4270 nm	CO_2	94 ppb	
DFB laser	Optical microphone	100 s	1532.83 nm	C_2H_2	9 ppb	[85]
			1650.96 nm	CH_4	37 ppb	
IR radiation source			3355 nm	C_2H_6	17 ppb	
			10,690 nm	C_2H_4	6 ppb	
			4690 nm	CO	4 ppb	
			4270 nm	CO_2	60 ppb	
DFB laser	Capacitive microphone	/	1520 nm	C_2H_2	/	[86]
			1654 nm	CH_4	/	
DFB laser	Optical microphone	1 s	1531.6 nm	C_2H_2	0.27 ppm	[87]
			1568.4 nm	CO	23.42 ppm	
DFB laser	Capacitive microphone	/	1531.6 nm	C_2H_2	0.5 ppm	[58]
			1650.9 nm	CH_4	3 ppm	
IR radiation source			3350 nm	C_2H_6	3 ppm	
			10500 nm	C_2H_4	3 ppm	
			4700 nm	CO	30 ppm	
			4300 nm	CO_2	100 ppm	
DFB laser	/	/	1522.1 nm	C_2H_2	383 ppb	[88]
			1653.7 nm	CH_4	2.83 ppm	

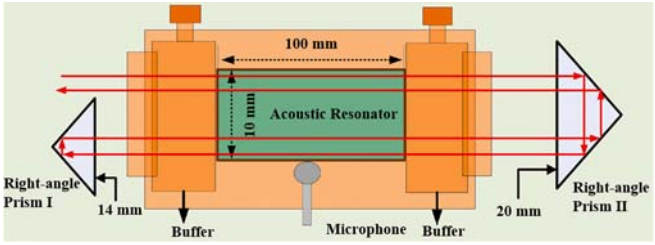

Fig. 5. Structural diagram of a multi-pass retro-reflection-cavity-enhanced PA cell [56].

radiation source with six filters were used to detect six decomposition gases. The results reveal that the average deviation between the concentration of each component extracted and the actual concentration is within 5 %, which indicates that the PAS has the potential to simultaneously detect multiple decomposition gases in transformer oil. In a recent study, Gong *et al.* developed a CF_4 PA detection system based on a

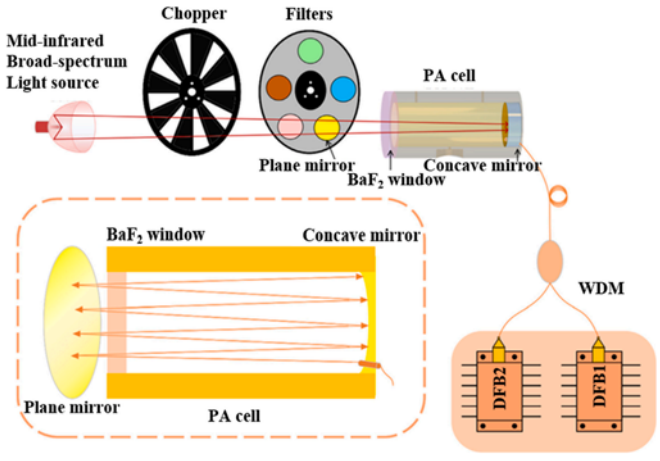

Fig. 6. Structural diagram of a multi-pass absorption-enhanced PA system [58].

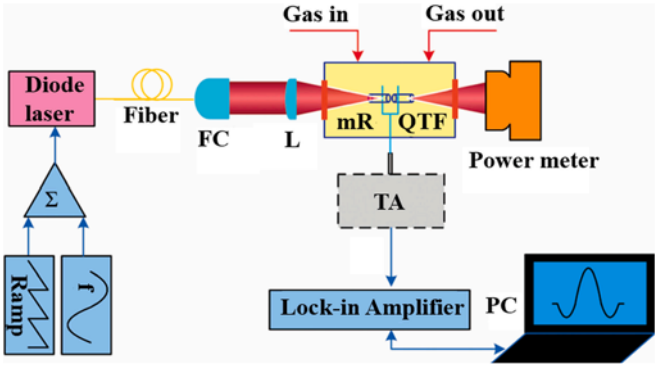

Fig. 7. Schematic diagram of a QEPAS system [59].

T-type PA cell, a cantilever diaphragm-based fiber optic F-P acoustic sensor, and a DFB laser [62]. The schematic diagram and actual photo of the all-optical high-sensitivity resonant PA sensor are shown in Fig. 8. Demodulation of the PA signal was carried out using fiber white light interferometry (WLI) [63]. The fiber-optic WLI-based demodulation approach benefits from the utilization of absolute measurements and is impervious to fluctuations in optical signal intensity due to its reliance on the fringe level and phase information of the collected spectrum.

4. Applications of PAS to fault diagnostics in SF_6 gas-insulated equipment

4.1. Fault diagnosis of SF_6 gas-insulated equipment

Since the 1960s, sulfur hexafluoride (SF_6) has been widely used as an insulating medium in gas-insulated equipment for high-voltage transmission lines and substations due to its exceptional ability to extinguish arcs and provide insulation [89]. At present, power systems consume 80 % of the total SF_6 production [90]. SF_6 gas-insulated equipment (gas-insulated switchgear (GIS), gas-insulated cable (GIC), gas-insulated transformer (GIT), and gas-insulated breaker (GIB)) has a smaller footprint, safer and more reliable operation, lower electrical radiation, longer service life, and easier on-site installation than traditional air insulation equipment [91–93]. Despite the requirement for multiple inspections prior to utilization, SF_6 gas-insulated equipment is nonetheless susceptible to insulation failures [94]. Faults in SF_6 gas-insulated equipment fall into the same categories as oil-immersed power transformers: electrical, thermal, and mechanical. Figs. 9 and 10 show the causes of various defects and the currently more often used diagnostic techniques, respectively [10,95].

With the benefit of anti-electromagnetic interference, DCA (decomposition component analysis) fault diagnosis is proposed as a means of evaluating the operational state of SF6 gas-insulated equipment, akin to DGA fault detection in transformer oil [96]. Attribute to the occurrence of failures, SF_6 can decompose into low fluorine sulfides (SF_x, x = 1, 2, 3, 4, and 5), but soon combines with F atoms to revert to SF_6 in the absence of impurities. However, due to the presence of molecular oxygen, water vapor, metallic materials, and solid insulation materials, SF_x further reacts with impurities to form stable by-products (SO_2F_2, SOF_2, SO_2, HF, H_2S, and other gases) [97]. The formation of major decomposition products is shown in Fig. 11 and the major decomposition products generated by different failure types are listed in Table 4. Some of these decomposition products, such as SOF_2 and SO_2F_2, are corrosive and toxic, posing serious hazards to stability of equipment operation and safety of personnel performing operations and maintenance [98]. Additionally, at low temperatures, SF_6 decomposition products are incapable of recombining independently to the original SF_6 molecules, which reduces SF_6 concentration and speeds up the degradation of SF_6 insulation [99]. Numerous studies have shown that the composition and formation rate of SF_6 decomposition products correspond to the severity and type of insulation defects. The decomposition characteristics of SF_6 resulting from thermal failure at temperatures lower than 400 °C were examined by Zeng et al. [100]. They found that H_2S only appeared at temperatures above 360 °C, which can be used as a characteristic gas for diagnosing thermal faults. When the temperature is between 300 and 400 °C, the proportion of CO_2, SOF_2 and SO_2 in the decomposition gas can reach 97 %. It was found by Ding *et al.* that the concentration ratio of (SOF_2 + SO_2)/(SO_2F_2) can be used to determine the type of discharge [101]. The ratio is 0–1 under corona discharge and 1–5 under spark discharge. Additionally, it was noted that during corona and spark discharges, the levels of the primary stable gases (SOF_2, SO_2F_2, and SO_2) rose in proportion to the dissipation of the discharge energy. Experiments by Tang *et al.* proved that concentration ratios of CF_4/CO_2, CF_4/SO_2, CO_2/SOF_2, and CO_2/ (CF_4 + CO_2) can be used to effectively diagnose the severity of PD [102].

Precise measurement of SF_6 decomposition products is conducive to evaluating the severity and nature of insulation faults, enabling timely maintenance of SF_6 insulation equipment. An online detection instrument for SF_6 decomposition products needs to comply with the following conditions: (1) only one sampling port; (2) small volume of gas cell; (3) multi-gas detection; (4) high sensitivity detection [103]. PAS with the above conditions has many application cases in SF_6 decomposition gas detection. The characteristics of SF_6 decomposition gas detection is that the SF_6 concentration in gas-insulated equipment usually exceeds 99.8 %, and physical properties of SF_6 are different from those of N_2 and air, so the detection of trace decomposition gases should be carried out in pure SF_6 buffer gas instead of air or N_2 as usual. In the field of literature, IR light sources were commonly used for detecting

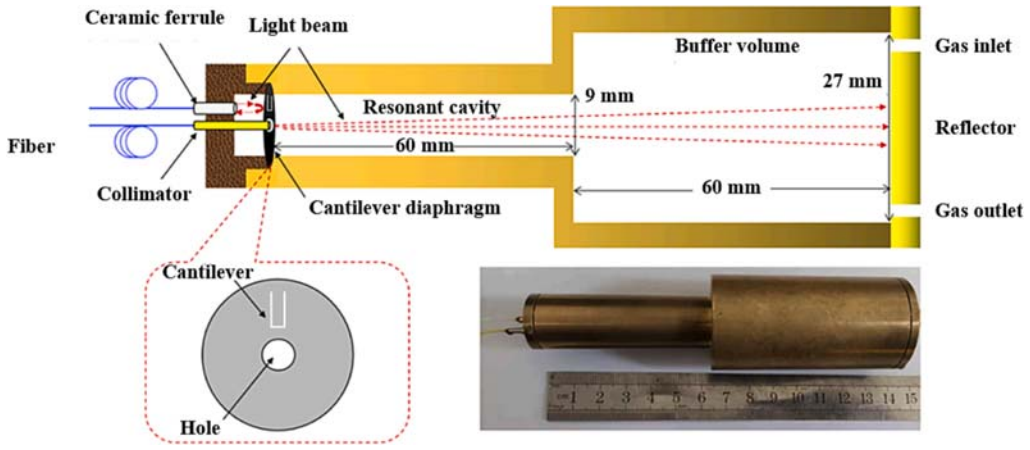

Fig. 8. Schematic diagram and photo of the all-optical PA sensor [62].

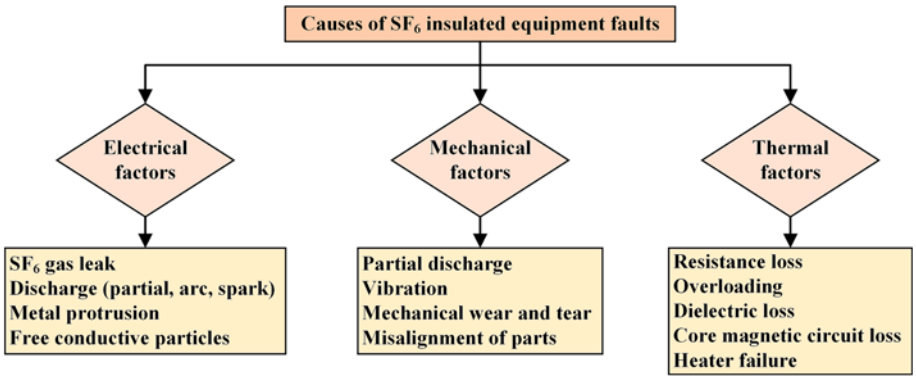

Fig. 9. Causes of faults in SF_6 insulated equipment.

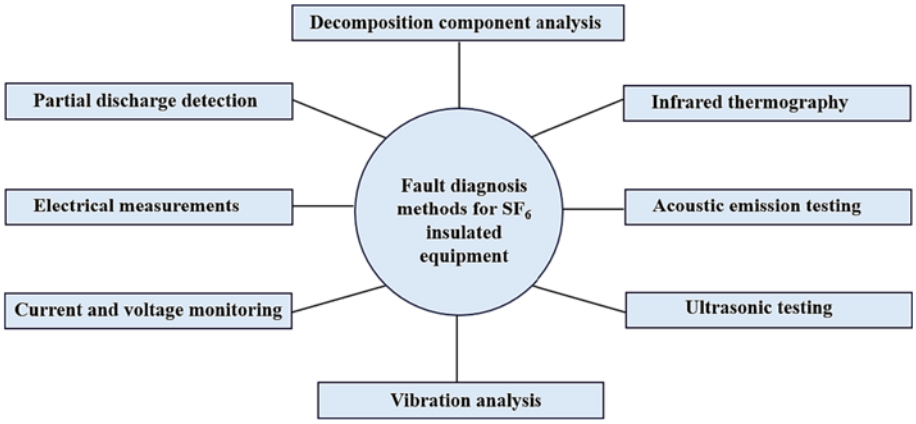

Fig. 10. Fault diagnosis methods for SF_6 insulated equipment.

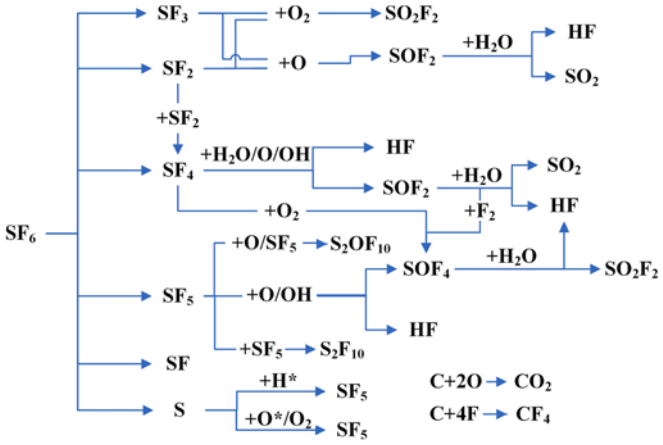

Fig. 11. Diagram of SF_6 gas decomposition process.

Table 4
Major SF_6 decomposition products generated by different failure types.

Fault type	Typical SF_6 decomposition products	Ref.
Arc	SOF_2, SO_2F_2, SF_4, SF_2, CF_4, and SOF_4	[106]
Spark	SOF_2, SO_2F_2, S_2F_2, SF_4, S_2F_{10}, $S_2F_{10}O$, SO_2, SOF_4, HF, CO_2, and CF_4	[107]
Partial discharge	SOF_2, SO_2F_2, SOF_4, SF_2, S_2F_2, S_2F_{10}, SF_4, SO_2, SOF_4, CF_4, CO_2, and HF	[101]
Thermal fault	CO_2, SO_2, SOF_4, SO_2F_2, SOF_2, and H_2S	[100]

decomposition gases, with the exception of SO_2 molecules which require an ultraviolet (UV) light source. This is because SF_6 molecules do not absorb light in the 250–400 nm [104] spectral region, while SO_2 has a strong line intensity in this range. Absorption spectra of SF_6 decomposition products in the IR regions are shown in Fig. 12 (from HITRAN database [54]), and the absorption spectrum of SO_2 between 170 nm and 325 nm is shown in Fig. 13(a) [104]. SOF_2 gas does not currently appear in any database, the IR spectrum derived from experimental measurements is shown in Fig. 13(b) [105]. Similar to PAS in the analysis of dissolved gas in insulation oil, Tables 5 and 6 summarize the application research of PAS in the field of SF_6 decomposition gas in recent years, based on single gas detection and multiple gas detection, respectively.

4.2. *PAS for fault diagnosis of SF_6 gas-insulated equipment*

4.2.1. *Traditional photoacoustic spectroscopy*

Lin *et al.* reported the detection of four SF_6 decomposition products (SO_2F_2, SO_2, CF_4, and CO_2) using a cylindrical PA cell and a broadband IR radiation source with a spectral range of 1–20 μm and detection limits of a few ppm [108]. GC–MS was used as the reference system to assess the performance of the PAS system. However, they did not consider the problem of spectral interference between interfering gases and decomposition gases [109]. Three SF_6 decomposition gases were simultaneously detected by Yin *et al.* using one UV laser and two DFB lasers. A dual-channel PA cell is composed of two identical cylindrical resonators, one of which is coupled to a UV laser and the other to two DFB lasers. The reported SF_6 decomposition gas detection system is capable of detecting gases at sub-ppm levels [109]. In a recent study, Wei *et al.* measured the concentrations of SO_2F_2, SO_2, and CF_4 using a widely tunable laser (external cavity QCL) (Fig. 14) [110]. By replacing the

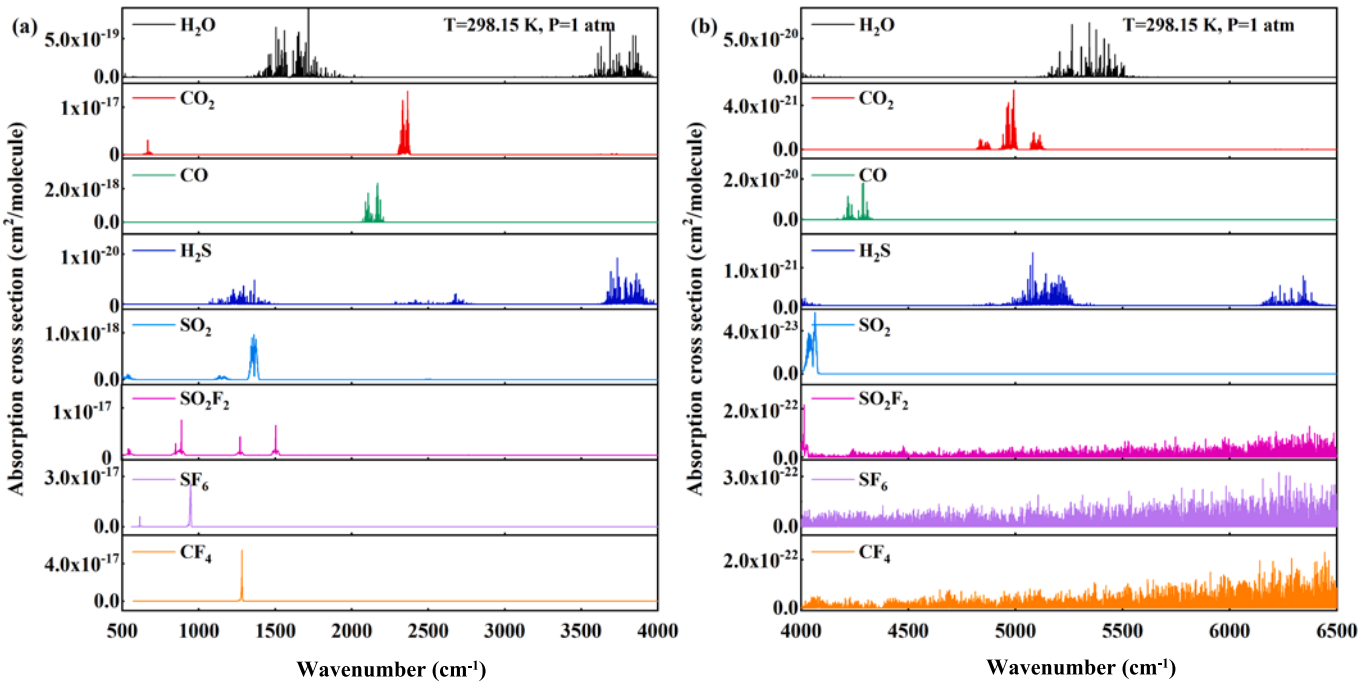

Fig. 12. Absorption spectra of SF_6 decomposition gases and water vapor in the mid-IR (a) and near-IR (b).

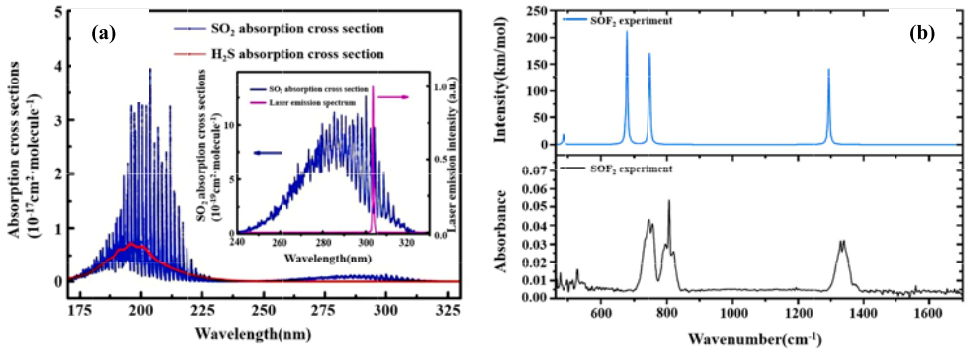

Fig. 13. (a) The absorption spectra of SO_2 and H_2S in the UV spectral region [104]. (b) The simulated IR absorption lines and experimentally measured IR absorption spectrum of SOF_2 [105].

Table 5
Applications of PAS to single-gas detection in the SF_6 gas-insulated equipment.

Gas	Light source	Acoustic sensor	Wavelength	Detection limit	Integration time	Ref.
H_2S	DFB laser	Optical microphone	1578 nm	1.75 ppm	/	[117]
	DFB laser	Optical microphone	1574.56 nm	0.15 ppm	1 s	[118]
	DFB laser	Optical microphone	1574.56 nm	197.2 ppb	1 s	[115]
	DFB laser	Capacitive microphone	1582 nm	109 ppb	1 s	[119]
SO_2	DPSSL	Capacitive microphone	303.6 nm	74 ppb	1 s	[104]
	Q-switching laser diode (LD)	Capacitive microphone	266 nm	140 ppb	1 s	[120]
	LED	Optical microphone	285 nm	0.667 ppm	/	[121]
CO	DFB laser	Optical microphone	1567.324 nm	9.88 ppm	/	[122]
	QCL	QTF	4610 nm	10 ppb	10 s	[112]
	DFB laser	Optical microphone	2.33 um	5.1 ppm	/	[116]
	DFB laser	Capacitive microphone	2330 nm	1.18 ppm	1 s	[123]
	DFB laser	Capacitive microphone	2330.2 nm	20.5 ppm	/	[124]
	DFB laser	Capacitive microphone	1166.3 nm	110 ppb	1 s	[125]
H_2O	DFB laser	QTF	1368 nm	0.49 ppm	1 s	[113]

Table 6
Applications of PAS to multi-gas detection in the SF_6 gas-insulated equipment.

Light source	Acoustic sensor	Integration time	Wavelength	Gas	Detection limit	Ref.
IR radiation source	Capacitive microphone	3 s	6644 nm 7353 nm 4241 nm 7825 nm	SO_2F_2 SO_2 CO_2 CF_4	0.45 ppm 0.26 ppm 0.1 ppm 0.245 ppm	[108]
IR radiation source	Capacitive microphone	/	7370 nm 4700 nm 7780 nm	SO_2 CO CF_4	8.2824 ppm 5.9116 ppm 5.5226 ppm	[25]
IR radiation source	Capacitive microphone	1 s	7350 nm 4260 nm 7780 nm	SO_2 CO_2 CF_4	3.6 ppm 5.7 ppm 7.6 ppm	[126]
DPSSL DFB laser	Capacitive microphone	1 s	303.6 nm 1568.1 nm 1572.1 nm	SO_2 CO H_2S	115 ppb 435 ppb 89 ppb	[109]
DFB laser	Optical microphone	/	1567.13 nm 1577.86 nm	CO H_2S	/ (N_2 buffer gas) / (N_2 buffer gas)	[114]
QCL	Capacitive microphone	95 s 147 s 107 s	7795 nm 7794 nm 7416 nm	SO_2F_2 CF_4 SO_2	70 ppb 1.5 ppb 7 ppb	[110]
QCL	Capacitive microphone	/	6648 nm 7460 nm	SO_2F_2 SOF_2	0.22 ppm (N_2 buffer gas) 0.28 ppm (N_2 buffer gas)	[111]

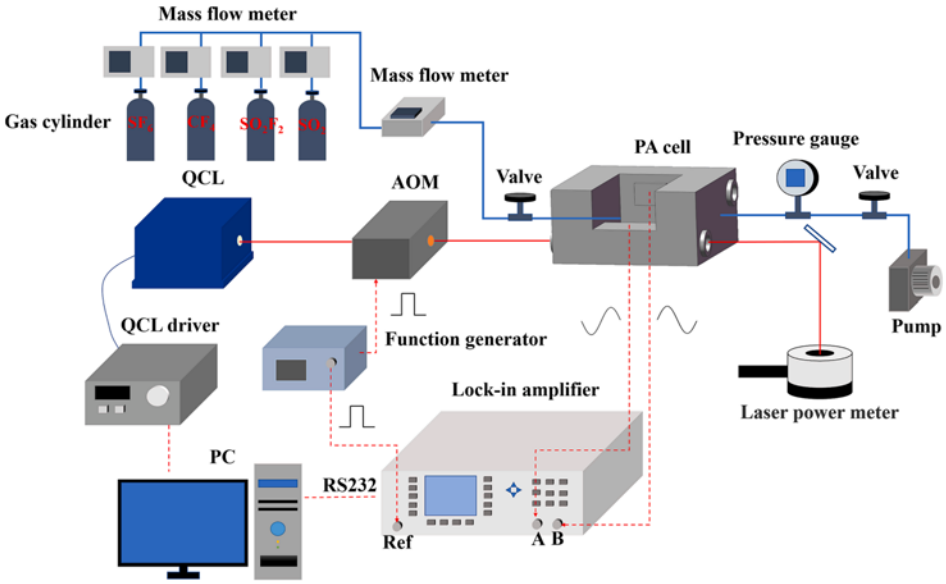

Fig. 14. PAS for detection of SF_6 decomposition by-products [110].

mechanical chopper with an acousto-optic modulator for intensity modulation, the mechanical noise created by the chopper was eliminated. A multiple linear regression (MLR) technique based on the least squares approach was used to resolve the spectra of the three gases, taking into account the cross-interference of the absorption spectra of the gases in the measurement band. Ultimately, with a measurement error of less than 4 %, detection limits of 70, 1.5, and 7 ppb for SO_2F_2, CF_4, and SO_2 were reached. Zhang *et al.* used two DFB-QCLs and an H-type PA cell to realize the detection of SO_2F_2 and SOF_2 [111]. Despite achieving a minimum detection limit of sub-ppm, the background absorption of SF_6 was not considered.

4.2.2. Quartz enhanced photoacoustic spectroscopy

A QEPAS system for the detection of CO_2 in SF_6 was developed by Sun *et al.* [112]. They used an optimized QTF with a resonant frequency of 8000 Hz instead of the conventional QTF because the vibration-translational energy transfer rate of CO could not adapt to the resonant frequency of conventional QTFs, which would lead to a weaker QEPAS signal. Finally, such a system achieved real-time monitoring of SF_6 decomposition by-products. Water vapor is an important factor leading to the generation of SF_6 decomposition gas. Yin *et al.* designed a QEPAS-based humidity sensor shown in Fig. 15 [113]. The study details the optimization of the sensor system, including aspects like resonant frequency, Q-factor, optimal laser beam position, and geometrical

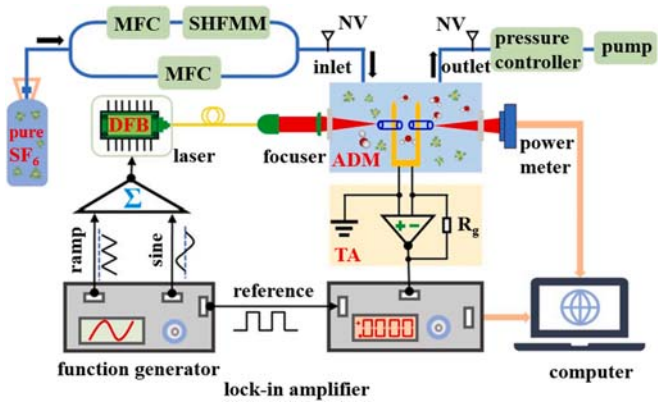

Fig. 15. QEPAS for detection of humidity in SF_6 buffer gas [113].

parameters of the acoustic micro-resonator. To humidify SF_6 gas in the experiment, a silicone hollow fiber membrane module was used behind a mass flow controller, enabling the adjustment of humidity levels by controlling gas flow rates. The humidity sensor achieved a NNEA of 1.59 $\times$ 10^{-7} $Wcm^{-1}Hz^{-1/2}$, making it adequately sensitive for monitoring humidity in high-voltage gas power systems.

4.2.3. All-optical photoacoustic spectroscopy

The work of Dai *et al.* was devoted to developing a PAS detection system that combines two lasers and a cantilever for simultaneous detection of H_2S and CO [114]. The modulation frequencies of the two lasers are 20 Hz and 40 Hz, respectively. The two laser beams are combined and introduced into the PA cell using a beam combiner. The PA signals of the two gases can be well distinguished in the frequency domain. Nevertheless, this experiment was only conducted using N_2 as the background, and it is anticipated that a subsequent experiment will be conducted with SF_6 as the background. In the study by Chen *et al.*, a cantilever-based fiber optic F-P acoustic sensor (Fig. 16) was used as a detection module for the acoustic signal of H_2S in SF_6 [115]. SF_6 and N_2 were used to simulate the resonance frequency of the H-type PA cell, and the difference in resonance frequency was about 2.5 times due to the differences in their physical properties. As a result of the Allan deviation analysis, when the integration time is 200 s, the minimum detection limit of H_2S in the SF_6 background reaches 14 ppb. Chen *et al.* used cantilever-enhanced PAS to detect CO at 4291.5 cm^{-1} [116]. Michelson interferometer is used to determine the deformation of the cantilever caused by the sound waves. The acoustic sensor is mounted in the middle of a non-resonant cylindrical PA resonator with an optimum

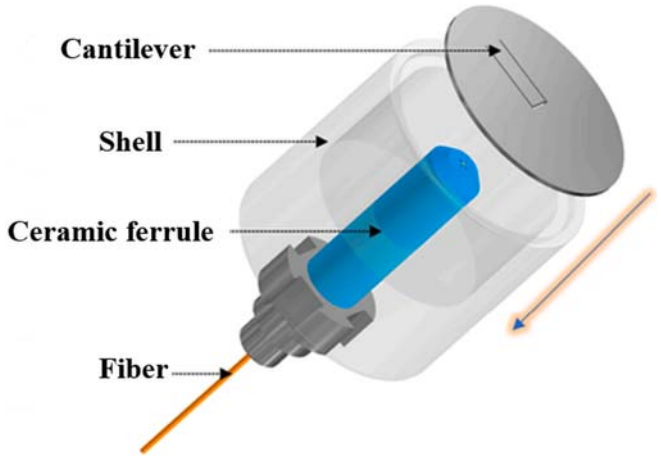

Fig. 16. Schematic diagram of the cantilever-based fiber optic F-P acoustic sensor [115].

modulation of 40 Hz. In the present study, the PA signal was detected at a concentration of 2000 ppm CO in the presence of four distinct background gases (SF_6, N_2, helium (He), and argon (Ar)). The results indicate variations in PA cell constants among different background gases. Furthermore, these constants exhibit a negative correlation with thermal conductivity, while showing a positive correlation with specific heat capacity, heat capacity at constant pressure, and background gas density.

5. Conclusion and future perspectives

In this review, we have explored the significant potential of PAS in the fault diagnostics of high-voltage power transmission systems. PAS, with its high selectivity, wide dynamic range, on-site and real-time operability, and strong anti-interference ability, stands as a promising diagnostic tool, particularly in the detection of decomposition gases in oil-immersed power transformers and SF_6 insulated equipment. The review underscores the current capabilities of PAS in accurately detecting a range of key gases like C_2H_2, CH_4, C_2H_6, CO_2, C_2H_4, and CO with sensitivities at the ppb level, which is significantly lower than their maximum concentrations in insulating oil. This sensitivity to gas compositions, especially the critical detection of C_2H_2, is pivotal in identifying high-energy discharge faults, which pose severe risks to equipment functionality and safety. Furthermore, we have discussed the applications of PAS in SF_6 decomposition gas detection and the related challenges, including the lack of standard absorption spectrum databases and technical standards for diagnosis.

Looking ahead, the path for PAS in this field involves several key directions. Firstly, enhancing the sensitivity and selectivity of PAS for a wider array of gases (mainly for SF_6 decomposition gas) is crucial. This may involve expanding the spectral range of detection to the UV and THz ranges and integrating PAS with other sensing technologies, like online H_2 sensors, for more comprehensive diagnostics. Another significant future avenue is the development of compact, commercially viable PAS systems that can be integrated into actual insulation systems for real-time monitoring. The miniaturization and robustness of these systems will be critical in facilitating their widespread field application. Additionally, establishing standard methods for interpreting DGA data and addressing the challenges of diagnosing faults based on decomposition gas analysis are vital for advancing the field. Furthermore, as we move towards more environmentally sustainable practices, analyzing the chemical reactions and fault diagnostics in alternative gases to SF_6 using PAS will be an emerging research direction. Addressing the uncertainties in the behavior of these alternative gases under fault conditions will contribute significantly to reducing the greenhouse impact of power transmission systems.

In summary, PAS is poised to significantly impact the fault diagnostics of high-voltage power transmission systems. Its evolution, marked by technological advancements and integration with other diagnostic methods, will not only enhance the accuracy and reliability of fault detection but also contribute to the sustainable management of power transmission networks. The path forward involves addressing current limitations, exploring new avenues of application, and standardizing methodologies, ensuring that PAS remains at the forefront of innovation in this critical field.

Funding

This work was supported by NSAF Joint Fund [U1830132], the National Key R&D Program of China [2019YFE0118200], and the National Natural Science Foundation of China (NSFC) [62175137].

CRediT authorship contribution statement

Qianhe Wei: Writing – original draft, Software, Investigation. **Bincheng Li:** Writing – review & editing, Supervision. **Binxing Zhao:**

Validation, Supervision. **Ping Yang:** Resources. **Lei Dong:** Funding acquisition.

Declaration of competing interest

The authors declare that they have no known competing financial interests or personal relationships that could have appeared to influence the work reported in this paper.

Data availability

No data was used for the research described in the article.

References

[1] J. Vijaychandra, B.R.V. Prasad, V.K. Darapureddi, B.V. Rao, Ł. Knypiński, A review of distribution system state estimation methods and their applications in power systems, Electronics 12 (2023) 603, https://doi.org/10.3390/electronics12030603.

[2] M.R. Hussain, S.S. Refaat, H. Abu-Rub, Overview and partial discharge analysis of power transformers: a literature review, IEEE Access 9 (2021) 64587–64605, https://doi.org/10.1109/access.2021.3075288.

[3] A.J. Christina, M.A. Salam, Q.M. Rahman, F. Wen, S.P. Ang, W. Voon, Causes of transformer failures and diagnostic methods - A review, Renew. Sustain. Energy Rev. 82 (2018) 1442–1456, https://doi.org/10.1016/j.rser.2017.05.165.

[4] J.S. N'Cho, I. Fofana, Y. Hadjadj, A. Beroual, Review of physicochemical-based diagnostic techniques for assessing insulation condition in aged transformers, Energies 9 (2016), https://doi.org/10.3390/en9050367.

[5] S. Chakravorti, D. Dey, B. Chatterjee, Recent trends in the condition monitoring of transformers: theory, implementation and analysis, (2013). doi: 10.1007/978-1-4471-5550-8.

[6] D. Lopez-Perez, J. Antonino-Daviu, Application of infrared thermography to failure detection in industrial induction motors: case stories, IEEE Trans. Ind. Appl. 53 (2017), https://doi.org/10.1109/TIA.2017.2655008.

[7] D. Zmarzly, T. Boczar, P. Fracz, S. Borucki, High voltage power transformer diagnostics using vibroacoustic method, in: 2014 IEEE International Power Modulator and High Voltage Conference, 2014, doi: 10.1109/IPMHVC.2014.7287337.

[8] R. Soni, B. Mehta, Diagnosis and prognosis of incipient faults and insulation status for asset management of power transformer using fuzzy logic controller & fuzzy clustering means, Electr. Pow. Syst. Res. 220 (2023) 109256, https://doi.org/10.1016/j.epsr.2023.109256.

[9] A. Rangel Bessa, J. Farias Fardin, P. Marques Ciarelli, L. Frizera Encarnação, Conventional dissolved gases analysis in power transformers: review, Energies 16 (2023) 7219, https://doi.org/10.3390/en16217219.

[10] V.Y. Ushakov, A.V. Mytnikov, I.U. Rakhmonov, Diagnostics of high voltage equipment, in: V.Y. Ushakov, A.V. Mytnikov, I.U. Rakhmonov (Eds.), High-Voltage Equipment of Power Systems: Design, Principles of Operation, Testing, Monitoring and Diagnostics, Springer Nature, Switzerland, Cham, 2023, https://doi.org/10.1007/978-3-031-38252-9_10.

[11] A.S. Mahdi, Z. Abdul-Malek, R.N. Arshad, SF_6 decomposed component analysis for partial discharge diagnosis in GIS: a review, IEEE Access 10 (2022) 27270–27288, https://doi.org/10.1109/access.2022.3156926.

[12] S.-A.-E.-S. Ward, S.A. Ibrahim, A. EL-Faraskoury, D.-E.A. Mansour, M. Badawi, Identification of transformer oil incipient faults based on the integration between different DGA techniques, Delta Univ. Sci. J. 6 (2023) 412–421, https://doi.org/10.21608/dusj.2023.291093.

[13] H. Syafruddin, H.P. Nugroho, Dissolved gas analysis (DGA) for diagnosis of fault in oil-immersed power transformers: a case study, in: 2020 4rd International Conference on Electrical, Telecommunication and Computer Engineering, 2020, doi: 10.1109/ELTICOM50775.2020.9230491.

[14] X. Zhang, B. Yang, X. Wang, C. Luo, Effect of plasma treatment on multi-walled carbon nanotubes for the detection of H_2S and SO_2, Sensors (Basel) 12 (2012) 9375–9385, https://doi.org/10.3390/s120709375.

[15] D.E. Matthews, J.M. Hayes, Isotope-ratio-monitoring gas chromatography-mass spectrometry, Anal. Chem. 50 (1978) 1465–1473, https://doi.org/10.1021/ac50033a022.

[16] N. Phansiri, X. Liu, K. Miwa, M. Inaba, M. Nakano, J. Suehiro, H. Sato, Indirect detection of residual CF_4 in gas-insulated switchgear via conversion under dielectric barrier discharge, Int. J. Plasma Environ. Sci. Technol. 15 (2021), https://doi.org/10.34343/ijpest.2021.15.e02010.

[17] D.C. Dumitras, M. Petrus, A.M. Bratu, C. Popa, Applications of near infrared photoacoustic spectroscopy for analysis of human respiration: a review, Molecules 25 (2020) 25, https://doi.org/10.3390/molecules25071728.

[18] Z. Wang, H. Zhang, Q. Wang, S. Borri, I. Galli, P. De Natale, et al., Doubly resonant sub-ppt photoacoustic gas detection with eight decades dynamic range, (2021), doi: 10.21203/rs.3.rs-431688/v1.

[19] X. Yin, Y. Su, T. Xi, B. Chen, L. Zhang, X. Zhang, et al., Research progress on photoacoustic SF_6 decomposition gas sensor in gas-insulated switchgear, J. Appl. Phys. 131 (2022), https://doi.org/10.1063/5.0089426.

[20] A.G. Bell, On the production and reproduction of sound by light, Am. J. Sci. s3–20 (1880) 305, https://doi.org/10.2475/ajs.s3-20.118.305.

[21] C. Haisch, Photoacoustic spectroscopy for analytical measurements, Meas. Sci. Technol. 23 (2012), https://doi.org/10.1088/0957-0233/23/1/012001.

[22] A. Sampaolo, P. Patimisco, M. Giglio, A. Zifarelli, H. Wu, L. Dong, V. Spagnolo, Quartz-enhanced photoacoustic spectroscopy for multi-gas detection: a review, Anal. Chim. Acta 1202 (2022) 338894, https://doi.org/10.1016/j.aca.2021.338894.

[23] P. Patimisco, G. Scamarcio, F.K. Tittel, V. Spagnolo, Quartz-enhanced photoacoustic spectroscopy: a review, Sensors 14 (2014) 6165–6206, https://doi.org/10.3390/s140406165.

[24] A. Fathy, Y.M. Sabry, I.W. Hunter, D. Khalil, T. Bourouina, Direct absorption and photoacoustic spectroscopy for gas sensing and analysis: a critical review, Laser Photonics Rev. 16 (2022), https://doi.org/10.1002/lpor.202100556.

[25] J. Luo, Y.H. Fang, Y.D. Zhao, A.J. Wang, D.C. Li, Y.Y. Li, Y. Liu, F.X. Cui, J. Wu, J. X. Liu, Research on the detection of SF_6 decomposition products based on non-resonant photoacoustic spectroscopy, Anal. Methods 7 (3) (2015) 1200–1207, https://doi.org/10.1039/C4AY02648A.

[26] Z.C. Luo, F.Y. Han, B. Tang, L.F. Zhang, C.Y. Liu, Q.Q. Liang, et al., Optical properties and decomposition mechanisms of SF_6 at different partial discharge determined by infrared spectroscopy, AIP Adv. 8 (2018) 065107, https://doi.org/10.1063/1.5030524.

[27] R. Lewicki, G. Wysocki, A.A. Kosterev, F.K. Tittel, QEPAS based detection of broadband absorbing molecules using a widely tunable, cw quantum cascade laser at 8.4 μm, Opt. Express 15 (2007) 7357–7366, https://doi.org/10.1364/OE.15.007357.

[28] A. Farooq, A.B.S. Alquaity, M. Raza, E.F. Nasir, S. Yao, W. Ren, Laser sensors for energy systems and process industries: perspectives and directions, Prog. Energy Combust. Sci. 91 (2022) 100997, https://doi.org/10.1016/j.pecs.2022.100997.

[29] F.J.M. Harren, S.M. Cristescu, Photoacoustic spectroscopy in trace gas monitoring, Encyclopedia Anal. Chem. (2019), https://doi.org/10.1002/9780470027318.a0718.pub3.

[30] M. Kwaśny, A.J.S. Bombalska, Optical methods of methane detection, Sensors 23 (2023) 2834, https://doi.org/10.3390/s23052834.

[31] J. Rouxel, J.-G. Coutard, S. Gidon, O. Lartigue, S. Nicoletti, B. Parvitte, et al., Miniaturized differential Helmholtz resonators for photoacoustic trace gas detection, Sens. Actuators B 236 (2016) 1104–1110, https://doi.org/10.1016/j.snb.2016.06.074.

[32] A.A. Kosterev, F.K. Tittel, D.V. Serebryakov, A.L. Malinovsky, I.V. Morozov, Applications of quartz tuning forks in spectroscopic gas sensing, Rev. Sci. Instrum. 76 (2005), https://doi.org/10.1063/1.1884196.

[33] T. Kuusela, J. Kauppinen, Photoacoustic gas analysis using interferometric cantilever microphone, Appl. Spectrosc. Rev. 42 (2007) 443–474, https://doi.org/10.1080/00102200701421755.

[34] B. Zoltan, P. Andrea, S. Gabor, Photoacoustic instruments for practical applications: present, potentials, and future challenges, Appl. Spectrosc. Rev. 46 (2011) 1–37, https://doi.org/10.1080/05704928.2010.520178.

[35] L. Jin, D. Kim, A. Abu-Siada, S. Kumar, Oil-immersed power transformer condition monitoring methodologies: a review, Energies 15 (2022) 3379, https://doi.org/10.3390/en15093379.

[36] V.A. Thiviyanathan, P.J. Ker, Y.S. Leong, F. Abdullah, A. Ismail, M. Zaini Jamaludin, Power transformer insulation system: a review on the reactions, fault detection, challenges and future prospects, Alex. Eng. J. 61 (2022) 7697–7713, https://doi.org/10.1016/j.aej.2022.01.026.

[37] M.M.F. Darwish, A. Samy, A.A. Abbas, D.E.A. Mansour, S.A. Ward, Impact of on-grid photovoltaic system on thermal performance of the oil-filled transformers, in: 2022 23rd International Middle East Power Systems Conference, 2022, doi: 10.1109/MEPCON55441.2022.10021729.

[38] M.M. Youssef, R.A. Ibrahim, H. Desouki, M.M.Z. Moustafa, An overview on condition monitoring & health assessment techniques for distribution transformers, in: 2022 6th International Conference on Green Energy and Applications, 2022, doi: 10.1109/ICGEA54406.2022.9791900.

[39] M. Gutten, M. Sebok, D. Korenciak, P. Brnčal, M. Kubis, P. Žukowski, et al., Frequency domain diagnostics of transformer insulation, devices and methods of measurements, 10 (2019) 353–359, doi: 10.21122/2220-9506-2019-10-4-353-359.

[40] U. Elele, A. Nekahi, A. Arshad, I. Fofana, Towards online ageing detection in transformer oil: a review, Sensors 22 (2022) 7923, https://doi.org/10.3390/s22207923.

[41] A.R. Abbasi, Fault detection and diagnosis in power transformers: a comprehensive review and classification of publications and methods, Electr. Pow. Syst. Res. 209 (2022), https://doi.org/10.1016/j.epsr.2022.107990.

[42] T. Boczar, A. Cichon, S. Borucki, Diagnostic expert system of transformer insulation systems using the acoustic emission method, IEEE Trans. Dielectr. Electr. Insul. 21 (2014) 854–865, https://doi.org/10.1109/TDEI.2013.004126.

[43] S.A. Ward, A. El-Faraskoury, M. Badawi, S.A. Ibrahim, K. Mahmoud, M. Lehtonen, M.M.F. Darwish, Towards precise interpretation of oil transformers via novel combined techniques based on DGA and partial discharge sensors, Sensors 21 (2021) 2223, https://doi.org/10.3390/s21062223.

[44] S.A. Ward, Dissolved gas analysis as diagnostic tool for evaluating the condition of the transformer, in: 13th International Symposium on High Voltage Engineering (ISH'03) 6629 (2003) S-263, doi: 10.1117/12.728476.

[45] A.J. Amalanathan, R. Sarathi, M. Zdanowski, R. Vinu, Z. Nadolny, Review on gassing tendency of different insulating fluids towards transformer applications, Energies 16 (2023) 488, https://doi.org/10.3390/en16010488.

[46] M. Meira, C. Ruschetti, R. Álvarez, L. Catalano, C. Verucchi, Dissolved gas analysis differences between natural esters and mineral oils used in power transformers: a review, 13 (2019) 5441–5448, doi: 10.1049/iet-gtd.2018.6318.

[47] S.A. Wani, A.S. Rana, S. Sohail, O. Rahman, S. Parveen, S.A. Khan, Advances in DGA based condition monitoring of transformers: a review, Renew. Sustain. Energy Rev. 149 (2021) 111347, https://doi.org/10.1016/j.rser.2021.111347.
[48] Z. Ayalew, K. Kobayashi, S. Matsumoto, M. Kato, Dissolved gas analysis (DGA) of arc discharge fault in transformer insulation oils (ester and mineral oils), in: 2018 IEEE Electrical Insulation Conference (EIC), 2018, doi: 10.1109/EIC.2018.8481123.
[49] A. Abu-Siada, M. Arshad, S. Islam, Fuzzy logic approach to identify transformer criticality using dissolved gas analysis, in: IEEE PES General Meeting, 2010, doi: 10.1109/PES.2010.5589789.
[50] E.A. Mackenzie, J. Crossey, A. Pablo, W. Ferguson, On-line monitoring and diagnostics for power transformers, in: 2010 IEEE International Symposium on Electrical Insulation, 2010, doi: 10.1109/ELINSL.2010.5549734.
[51] E.S.M. El-kenawy, F. Albalawi, S.A. Ward, S.S.M. Ghoneim, M.M. Eid, A. A. Abdelhamid, N. Bailek, A. Ibrahim, Feature selection and classification of transformer faults based on novel meta-heuristic algorithm, Mathematics 10 (2022) 3144, https://doi.org/10.3390/math10173144.
[52] M. Badawi, S.A. Ibrahim, A.E. Faraskoury, D.A. Mansour, S.A. Ward, A novel DGA oil interpretation approach based on combined techniques, in: 2022 23rd International Middle East Power Systems Conference, 2022, doi: 10.1109/MEPCON55441.2022.10021795.
[53] S.A. Ward, A. ELFaraskoury, M. Badwi, S.A. Ibrahim, A modified dissolved gas analysis technique as a diagnostic tool for faults in power transformers, in: 2019 21st International Middle East Power Systems Conference, 2019, doi: 10.1109/MEPCON47431.2019.9008209.
[54] I.E. Gordon, L.S. Rothman, R.J. Hargreaves, R. Hashemi, E.V. Karlovets, F. M. Skinner, et al., The HITRAN2020 molecular spectroscopic database, J. Quant. Spectrosc. Radiat. Transf. 277 (2022), https://doi.org/10.1016/j.jqsrt.2021.107949.
[55] Z. Wu, Y. Gong, Q. Yu, Photoacoustic spectroscopy detection and extraction of discharge feature gases in transformer oil based on 1.5μ tunable fiber laser, Infrared Phys. Technol. 58 (2013) 86–90, https://doi.org/10.1016/j.infrared.2013.01.002.
[56] Y. Ma, S. Qiao, Y. He, Y. Li, Z. Zhang, X. Yu, et al., Highly sensitive acetylene detection based on multi-pass retro-reflection-cavity-enhanced photoacoustic spectroscopy and a fiber amplified diode laser, Opt. Express 27 (2019) 14163–14172, https://doi.org/10.1364/OE.27.014163.
[57] G.Z. Wang, D.H. Fu, S. Yuan, C.X. Li, X. Han, J.C. Du, et al., Rapid detection of dissolved acetylene in oil based on T-type photoacoustic cell, Microw. Opt. Technol. Lett. (2023), https://doi.org/10.1002/mop.33793.
[58] C. Li, H. Qi, X. Zhao, M. Guo, R. An, K. Chen, Multi-pass absorption enhanced photoacoustic spectrometer based on combined light sources for dissolved gas analysis in oil, Opt. Lasers Eng. 159 (2022), https://doi.org/10.1016/j.optlaseng.2022.107221.
[59] Y.F. Ma, Y. Tong, L.G. Zhang, Y. He, J.B. Zhang, L. Wang, et al., Study on high sensitive detection of acetylene trace gas based on QEPAS, Spectrosc. Spectral Anal. 37 (2017) 2869–2872, https://doi.org/10.3964/j.issn.1000-0593(2017)09-2869-04.
[60] Q. Wang, J. Wang, L. Li, Q. Yu, An all-optical photoacoustic spectrometer for trace gas detection, Sens. Actuators B 153 (2011) 214–218, https://doi.org/10.1016/j.snb.2010.10.035.
[61] Z.F. Gong, K. Chen, Y. Yang, X.L. Zhou, Q.X. Yu, Photoacoustic spectroscopy based multi-gas detection using high-sensitivity fiber-optic low-frequency acoustic sensor, Sens. Actuator B-Chem. 260 (2018) 357–363, https://doi.org/10.1016/j.snb.2018.01.005.
[62] Z. Gong, G. Wu, X. Jiang, H. Li, T. Gao, M. Guo, et al., All-optical high-sensitivity resonant photoacoustic sensor for remote CH_4 gas detection, Opt. Express 29 (2021) 13600–13609, https://doi.org/10.1364/oe.424387.
[63] K. Chen, Z. Yu, Z. Gong, Q. Yu, Lock-in white-light-interferometry-based all-optical photoacoustic spectrometer, Opt. Lett. 43 (2018) 5038–5041, https://doi.org/10.1364/OL.43.005038.
[64] Q. Zhou, C. Tang, S. Zhu, W. Chen, X. Peng, Detection of dissolved carbon monoxide in transformer oil using 1.567 μm diode laser-based photoacoustic spectroscopy, J. Spectrosc. 2015 (2015) 737635, https://doi.org/10.1155/2015/737635.
[65] Q. Zhou, S. Peng, Q. Wang, G. Wu, W. Chen, Study of carbon monoxide detection characteristics with a tunable photoacoustic spectroscopy system, in: 2016 IEEE International Conference on High Voltage Engineering and Application, 2016, doi: 10.1109/ICHVE.2016.7800889.
[66] Z. Gong, K. Chen, Y. Yang, X. Zhou, W. Peng, Q. Yu, High-sensitivity fiber-optic acoustic sensor for photoacoustic spectroscopy based traces gas detection, Sens. Actuators B 247 (2017) 290–295, https://doi.org/10.1016/j.snb.2017.03.009.
[67] T.H. Yang, K. Zhou, L. Jin, R. Liu, W.G. Chen, Optimization of photoacoustic cell for trace acetylene detection in transformer oil, Atmos. 14 (2023), https://doi.org/10.3390/atmos14050801.
[68] Y. Cao, W. Jin, H.L. Ho, J. Ma, Miniature fiber-tip photoacoustic spectrometer for trace gas detection, Opt. Lett. 38 (2013) 434–436, https://doi.org/10.1364/OL.38.000434.
[69] M. Zhang, B. Zhang, K. Chen, M. Guo, S. Liu, Y. Chen, et al., Miniaturized multi-pass cell based photoacoustic gas sensor for parts-per-billion level acetylene detection, Sens. Actuators, A 308 (2020), https://doi.org/10.1016/j.sna.2020.112013.
[70] M. Guo, K. Chen, C. Li, L. Xu, G. Zhang, N. Wang, et al., High-sensitivity silicon cantilever-enhanced photoacoustic spectroscopy analyzer with low gas consumption, Anal. Chem. 94 (2022) 1151–1157, https://doi.org/10.1021/acs.analchem.1c04309.
[71] K. Chen, R. An, C. Li, Y. Kang, F. Ma, X. Zhao, et al., Detection of ultra-low concentration acetylene gas dissolved in oil based on fiber-optic photoacoustic sensing, Opt. Laser Technol. 154 (2022), https://doi.org/10.1016/j.optlastec.2022.108299.
[72] S. Zhou, D. Iannuzzi, Immersion photoacoustic spectrometer (iPAS) for arcing fault detection in power transformers, Opt. Lett. 44 (2019) 3741–3744, https://doi.org/10.1364/OL.44.003741.
[73] T. Chen, F. Ma, Y. Zhao, Y. Zhao, L. Wan, K. Li, et al., Portable ppb-level acetylene photoacoustic sensor for transformer on-field measurement, Optik 243 (2021), https://doi.org/10.1016/j.ijleo.2021.167440.
[74] C. Zhang, Q. Wang, X. Yin, Photoacoustic spectroscopy for detection of trace C_2H_2 using ellipsoidal photoacoustic cell, Opt. Commun. 487 (2021), https://doi.org/10.1016/j.optcom.2021.126764.
[75] H. Pan, Q. Wang, C. Zhang, Z. Li, P. Shan, Z. Ma, High-sensitivity acetylene detection system using ellipsoid multi-pass cell (EMPC) based on the opposite dual optical source, Infrared Phys. Technol. 118 (2021), https://doi.org/10.1016/j.infrared.2021.103874.
[76] K. Chen, Z. Gong, Q. Yu, Fiber-amplifier-enhanced resonant photoacoustic sensor for sub-ppb level acetylene detection, Sens. Actuators, A 274 (2018) 184–188, https://doi.org/10.1016/j.sna.2018.02.025.
[77] F. Ma, Z. Liao, Y. Zhao, Z. Qiu, L. Wan, K. Li, et al., Detection of trace C_2H_2 in N_2 buffer gas with cantilever-enhanced photoacoustic spectrometer, Optik 232 (2021) 166525, https://doi.org/10.1016/j.ijleo.2021.166525.
[78] Z. Gong, K. Chen, Y. Chen, L. Mei, Q. Yu, Integration of T-type half-open photoacoustic cell and fiber-optic acoustic sensor for trace gas detection, Opt. Express 27 (2019) 18222–18231, https://doi.org/10.1364/OE.27.018222.
[79] C. Yin, S. Jiang, Y. Zhang, A photoacoustic spectrum detection system based on chaos detection of weak signal, in: 2021 IEEE 5th Advanced Information Technology, Electronic and Automation Control Conference, 2021, doi: 10.1109/IAEAC50856.2021.9391119.
[80] Z. Gong, T. Gao, L. Mei, K. Chen, Y. Chen, B. Zhang, et al., Ppb-level detection of methane based on an optimized T-type photoacoustic cell and a NIR diode laser, Photoacoustics 21 (2021) 100216, https://doi.org/10.1016/j.pacs.2020.100216.
[81] Y. Yun, X. Zhao, Laser resonant photoacoustic spectrometer for methane detection, IOP Conf. Ser.: Earth Environ. Sci. 526 (2020), https://doi.org/10.1088/1755-1315/526/1/012075.
[82] T. Yang, W. Chen, Detection of dissolved gas in transformer oil based on all-optical photoacoustic spectroscopy, in: 2020 IEEE International Conference on High Voltage Engineering and Application, 2020, doi: 10.1109/ICHVE49031.2020.9279929.
[83] X. Mao, X. Zhou, L. Zhai, Q. Yu, Dissolved gas-in-oil analysis in transformers based on near-infrared photoacoustic spectroscopy, Int. J. Thermophys. 36 (2015) 940–946, https://doi.org/10.1007/s10765-014-1713-2.
[84] K. Chen, S. Liu, B. Zhang, Z. Gong, Y. Chen, M. Zhang, et al., Highly sensitive photoacoustic multi-gas analyzer combined with mid-infrared broadband source and near-infrared laser, Opt. Lasers Eng. 124 (2020), https://doi.org/10.1016/j.optlaseng.2019.105844.
[85] K. Chen, B. Zhang, M. Guo, H. Deng, B. Yang, Z. Gong, et al., All-optical photoacoustic multigas analyzer using digital fiber-optic acoustic detector, IEEE Trans. Instrum. Meas. 69 (2020) 8486–8493, https://doi.org/10.1109/tim.2020.2993333.
[86] Y. Yun, Q. Jiang, Multi-component gas photoacoustic detection, IOP Conf. Ser.: Earth Environ. Sci. 508 (2020) 012135, https://doi.org/10.1088/1755-1315/508/1/012135.
[87] H. Cheng, J. Tang, X. Zhang, Y. Li, J. Hu, Y. Zhang, et al., Simultaneous detection of C_2H_2 and CO based on cantilever-enhanced photoacoustic spectroscopy, IEEE Trans. Instrum. Meas. 70 (2021) 1–10, https://doi.org/10.1109/TIM.2021.3080377.
[88] X. Zhang, L. Liu, L. Zhang, H. Huan, L. Dong, Y. Zhou, et al., A compact, selective and embedded-system enabled photoacoustic sensor for multiple trace detection, in: 2021 Conference on Lasers and Electro-Optics, 2021, https://ieeexplore.ieee.org/document/9571793.
[89] A. Beroual, A. Haddad, Recent advances in the quest for a new insulation gas with a low impact on the environment to replace sulfur hexafluoride (SF6) gas in high-voltage power network applications, Energies 10 (2017), https://doi.org/10.3390/en10081216.
[90] M. Rabie, C.M. Franck, Assessment of eco-friendly gases for electrical insulation to replace the most potent industrial greenhouse gas SF_6, Environ. Sci. Tech. 52 (2018) 369–380, https://doi.org/10.1021/acs.est.7b03465.
[91] J. Owens, A. Xiao, J. Bonk, M. DeLorme, A. Zhang, Recent development of two alternative gases to SF_6 for high voltage electrical power applications, Energies 14 (2021) 5051, https://doi.org/10.3390/en14165051.
[92] C.M. Franck, A. Chachereau, J. Pachin, SF_6-free gas-insulated switchgear: current status and future trends, IEEE Electr. Insul. Mag. 37 (2021) 7–16, https://doi.org/10.1109/MEI.2021.9290463.
[93] M. El Bahy, S. Ward, R. Morsi, M. Badawi, Particle-initiated breakdown in gas-insulated co-axial configuration, in: 2011 Annual Report Conference on Electrical Insulation and Dielectric Phenomena, 2011, doi: 10.1109/CEIDP.2011.6232758.
[94] F. Zeng, H. Li, H. Cheng, J. Tang, Y. Liu, SF_6 decomposition and insulation condition monitoring of GIE: a review, High Voltage 6 (2021) 955–966, https://doi.org/10.1049/hve2.12160.
[95] W. Sima, Z. Yin, P. Sun, L. Li, Q. Shao, T. Yuan, et al., Thermal damage process and failure mechanism of epoxy/SF_6 composite insulation subjected to arc ablation, IEEE Trans. Dielectr. Electr. Insul. 27 (2020) 2014–2022, https://doi.org/10.1109/TDEI.2020.008858.

[96] Z. Cao, J. Tang, F. Zeng, Q. Yao, Y. Miao, SF6 positive DC partial discharge decomposition components under four typical insulation defects, IET Gener. Transm. Distrib. 13 (2018) 1–8, https://doi.org/10.1049/iet-gtd.2018.5101.
[97] S. Okabe, S. Kaneko, T. Minagawa, C. Nishida, Detecting characteristics of SF_6 decomposed gas sensor for insulation diagnosis on gas insulated switchgears, IEEE Trans. Dielectr. Electr. Insul. 15 (2008) 251–258, https://doi.org/10.1109/T-DEI.2008.4446758.
[98] C. Toigo, T. Vu-Cong, F. Jacquier, A. Girodet, Partial discharge behavior of protrusion on high voltage conductor in GIS/GIL under high voltage direct current: comparison of SF_6 and SF_6 alternative gases, IEEE Trans. Dielectr. Electr. Insul. 27 (2020) 140–147, https://doi.org/10.1109/TDEI.2019.008358.
[99] Y. Fu, M. Rong, K. Yang, A. Yang, X. Wang, Q. Gao, et al., Calculated rate constants of the chemical reactions involving the main byproducts SO_2F, SOF_2, SO_2F_2 of SF_6decomposition in power equipment, J. Phys. D Appl. Phys. 49 (2016) 155502, https://doi.org/10.1088/0022-3727/49/15/155502.
[100] F. Zeng, J. Tang, Q. Fan, J. Pan, X. Zhang, Q. Yao, et al., Decomposition characteristics of SF_6 under thermal fault for temperatures below 400°C, Dielectr. Electr. Insul. IEEE Trans. 21 (2014) 995–1004, https://doi.org/10.1109/TDEI.2014.6832242.
[101] W. Ding, G. Li, X. Ren, X. Yan, F. Li, W. Zhou, et al., A comparison of SF_6 decomposition characteristics under corona with point-to-plane electrode defect and spark with floating potential defect, IEEE Trans. Dielectr. Electr. Insul. 22 (2015) 3278–3289, https://doi.org/10.1109/TDEI.2015.004752.
[102] J. Tang, X. Yang, D. Yang, Q. Yao, Y. Miao, C. Zhang, et al., Using SF_6 decomposed component analysis for the diagnosis of partial discharge severity initiated by free metal particle defect, Energies 10 (2017), https://doi.org/10.3390/en10081119.
[103] X. Fan, L.i. Li, Y. Zhou, N. Tang, Z. Zou, X. Li, G. Huang, M. Liu, Online detection technology for SF_6 decomposition products in electrical equipment: a review, IET Sci. Meas. Technol. 12 (6) (2018) 707–711, https://doi.org/10.1049/iet-smt.2017.0573.
[104] X.K. Yin, L. Dong, H.P. Wu, H.D. Zheng, W.G. Ma, L. Zhang, et al., Highly sensitive SO_2 photoacoustic sensor for SF_6 decomposition detection using a compact mW-level diode-pumped solid-state laser emitting at 303 nm, Opt. Express 25 (2017) 32581–32590, https://doi.org/10.1364/oe.25.032581.
[105] C. Bian, F. Dai, J. Cheng, Q. Gan, Z. Zhang, G. Cui, et al., Analysis of infrared characteristics of SO_2F_2 and SOF_2 of SF_6 decomposition components, in: 2021 International Conference on Electrical Materials and Power Equipment, 2021, doi: 10.1109/ICEMPE51623.2021.9509100.
[106] I. Sauers, H.W. Ellis, L.G. Christophorou, Neutral decomposition products in spark breakdown of SF_6, IEEE Trans. Electr. Insul. EI-21 (1986) 111–120, doi: 10.1109/TEI.1986.348932.
[107] F.Y. Chu, SF_6 Decomposition in gas-insulated equipment, IEEE Trans. Electr. Insul. EI-21 (1986) 693–725, doi: 10.1109/TEI.1986.348921.
[108] T. Lin, G. Zhang, Z. Qiu, R. Guo, K. Li, D. Han, Photoacoustic detection of SF_6 decomposition by-products with broadband infrared source, in: 2014 International Conference on Power System Technology, 2014, doi: 10.1109/POWERCON.2014.6993837.
[109] X. Yin, L. Dong, H. Wu, L. Zhang, W. Ma, W. Yin, et al., Highly sensitive photoacoustic multicomponent gas sensor for SF6 decomposition online monitoring, Opt. Express 27 (2019) A224–A234, https://doi.org/10.1364/OE.27.00A224.
[110] Q. Wei, B. Li, B. Zhao, P. Yang, EC-QCL based photoacoustic spectroscopy for detection of SF_6 decomposition components, Sens. Actuators B 369 (2022), https://doi.org/10.1016/j.snb.2022.132351.
[111] Y. Zhang, M. Wang, P. Yu, Z. Liu, Optical gas sensing of sub-ppm SO_2F_2 and SOF_2 from SF_6 decomposition based on photoacoustic spectroscopy, IET Optoelectron. (2022), https://doi.org/10.1049/ote2.12077.
[112] B. Sun, A. Zifarelli, H. Wu, S. Dello Russo, S. Li, P. Patimisco, et al., Mid-Infrared quartz-enhanced photoacoustic sensor for ppb-level CO detection in a SF_6 gas matrix exploiting a T-grooved quartz tuning fork, Anal. Chem. 92 (2020) 13922–13929, https://doi.org/10.1021/acs.analchem.0c02772.
[113] X. Yin, L. Dong, H. Wu, M. Gao, L. Zhang, X. Zhang, et al., Compact QEPAS humidity sensor in SF_6 buffer gas for high-voltage gas power systems, Photoacoustics 25 (2022) 100319, https://doi.org/10.1016/j.pacs.2021.100319.
[114] F. Dai, C. Bian, J. Cheng, Q. Gan, X. Chen, Z. Zhang, Dual laser cantilever enhanced photoacoustic spectroscopy detection system for SF_6 decomposition components, in: 2020 IEEE 4th Conference on Energy Internet and Energy System Integration, 2020, doi: 10.1109/EI250167.2020.9346680.
[115] K. Chen, N. Wang, M. Guo, X. Zhao, H. Qi, C. Li, et al., Detection of SF_6 gas decomposition component H_2S based on fiber-optic photoacoustic sensing, Sens. Actuat. B 378 (2023) 133174, https://doi.org/10.1016/j.snb.2022.133174.
[116] Z. Chen, X. Zhang, T. Yang, S. Fan, H. Cheng, G. Xu, et al., Detection of trace carbon monoxide based on cantilever enhanced photoacoustic spectroscopy at 2.33 μm, Infrared Phys. Technol. 126 (2022), https://doi.org/10.1016/j.infrared.2022.104364.
[117] X.X. Zhang, Z. Cheng, X. Li, Cantilever enhanced photoacoustic spectrometry: quantitative analysis of the trace H_2S produced by SF6 decomposition, Infrared Phys. Technol. 78 (2016) 31–39, https://doi.org/10.1016/j.infrared.2016.07.004.
[118] M. Guo, X. Zhao, K. Chen, D. Cui, G. Zhang, C. Li, et al., Multi-mechanism collaboration enhanced photoacoustic analyzer for trace H(2)S detection, Photoacoustics 29 (2023) 100449, https://doi.org/10.1016/j.pacs.2023.100449.
[119] X. Yin, L. Dong, H. Wu, W. Ma, L. Zhang, W. Yin, et al., Ppb-level H_2S detection for SF_6 decomposition based on a fiber-amplified telecommunication diode laser and a background-gas-induced high-Q photoacoustic cell, Appl. Phys. Lett. 111 (2017), https://doi.org/10.1063/1.4987008.
[120] B. Chen, H. Li, X. Zhao, M. Gao, K. Cheng, X. Shao, et al., Trace photoacoustic SO_2 gas sensor in SF_6 utilizing a 266 nm UV laser and an acousto-optic power stabilizer, Opt. Express 31 (2023) 6974–6981, https://doi.org/10.1364/OE.483240.
[121] T. Chen, F. Ma, Y. Zhao, Z. Liao, Z. Qiu, G. Zhang, Cantilever enhanced based photoacoustic detection of SF_6 decomposition component SO_2 using UV LED, Sens. Rev. (2021), https://doi.org/10.1108/sr-12-2020-0292 ahead-of-print.
[122] H. Cheng, X. Zhang, C. Bian, J. Cheng, Z. Chen, Y. Zhang, et al., Photoacoustic spectroscopy: trace CO detection by using 10 mW near-infrared laser and cantilever beam, AIP Adv. 10 (2020), https://doi.org/10.1063/1.5134882.
[123] X.K. Yin, L. Dong, H.P. Wu, L.X. Liu, X.P. Shao, Design and optimization of photoacoustic CO gas sensor for fault diagnosis of SF6 gas insulated equipment, Acta Phys. Sin. 70 (2021), https://doi.org/10.7498/aps.70.20210532.
[124] Z. Chen, X. Zhang, H. Cheng, Y. Zhang, T. Yang, Y. Zhang, Study on Photoacoustic Spectroscopy Detection of CO in Gas Insulation Equipment, IEEE Trans. Dielectr. Electr. Insul. 29 (2022) 1498–1505, https://doi.org/10.1109/tdei.2022.3178059.
[125] X. Yin, H. Wu, L. Dong, W. Ma, L. Zhang, W. Yin, et al., Ppb-level photoacoustic sensor system for saturation-free CO detection of SF6 decomposition by use of a 10 W fiber-amplified near-infrared diode laser, Sens. Actuators B 282 (2019) 567–573, https://doi.org/10.1016/j.snb.2018.11.100.
[126] W. Cai, J. Tang, L. Cheng, C. Zhang, M. Fan, Q. Zhou, et al., Detection of SF_6 decomposition components under partial discharge by photoacoustic spectrometry and its temperature characteristic, IEEE Trans. Instrum. Meas. 65 (2016) 1343–1351, https://doi.org/10.1109/TIM.2013.2276474.